Photoinduced Intermolecular Electron Transfer in Liquid Solutions

V. O. Saik, A. A. Goun, J. Nanda,† Koichiro Shirota,‡ H. L. Tavernier, and M. D. Fayer*

Department of Chemistry, Stanford University, Stanford, California 94305

Received: February 10, 2004; In Final Form: April 22, 2004

Intermolecular photoinduced electron transfer between Rhodamine 3B cation ($R3B^+$), and dimethylanaline (DMA) is studied in a variety of solvents using pump−probe spectroscopy from ultrashort times (∼100 fs) to long times (∼10 ns). Excitation of $R3B^+$ results in the transfer of an electron from DMA and the production of the neutral radical R3B and the DMA^+ radical cation. Using a very broadband continuum probe, the generation of the R3B neutral radical is observed (430 nm) as well as the ground state bleach (550 nm), an excited state absorption (445 nm), and stimulated emission (620 nm). A good spectrum of the R3B radical is obtained by removing the overlapping excited state absorption. The forward electron transfer is examined by monitoring the time dependence of the stimulated emission. The data are analyzed with a previously presented detailed theory of through-solvent electron transfer for diffusing donors and acceptors, which includes the influences solvent structure and the hydrodynamic effect. Previous studies have shown that the theory works well for times >100 ps. It is found that in a non-hydrogen-bonding solvent (acetonitrile) and in mixtures of hydrogen-bonding solvents, the theory works well down to a few hundred femtoseconds with only one adjustable parameter, the contact electronic coupling matrix element. However, in pure hydrogen-bonding solvents, it is necessary to increase the solvent hard sphere radius used in the radial distribution to theoretically describe the data, which suggest a larger solvent structural unit than a single solvent molecule.

I. Introduction

The transfer of an electron from a donor to an acceptor is the fundamental step in a wide range of chemical and biological processes. As a result, electron-transfer reactions have been focus of numerous theoretical[1−6] and experimental[7−18] efforts aimed at understanding the kinetics and mechanism of the transfer event. Photoinduced electron transfer makes it possible to study electron transfer with a well-defined initiation time. In many cases, electron transfer takes place through bonds that link the donor to the acceptor.[19] However, in many other situations, the donor is not directly connected to an acceptor.[9,20,21] Electron transfer takes place because of the "through solvent" distance dependent intermolecular interactions that can couple the states of a donor and an acceptor.[1−6] The solvent may be a liquid,[7−10] a micelle,[11−15] or a protein.[16−18] The solvent is any medium in which the pathway for the electron transport is not directly through covalent bonds. Because the intermolecular interactions fall off steeply with distance, the spatial distribution of acceptors relative to a donor is critical in determining the rate and efficacy of electron transfer.[7,22]

Liquid solvents are an important medium for electron-transfer processes. Despite the ubiquity of liquid solvents, understanding the interplay of factors that influence photoinduced electron transfer between donors and acceptors in liquids remains a challenging problem. In the experiments described below as well as in other experiments,[9,20,21] a low concentration donor and high concentration acceptors are dissolved in a liquid. The time dependence of photoinduced electron transfer depends on the concentration of the species, the diffusion constants, and the distance dependence of the transfer rate. The distance dependence of the transfer rate depends on the strength of the electronic interaction, the free energy change upon electron transfer, and the reorganization energy.[1−6] Because the donors and acceptors are constantly moving through the liquid, their relative positions, and, therefore, the transfer rates, are not fixed. The transfer rate from a particular donor to the ensemble of acceptors is a complex function that depends on the position of the particles, the solvent properties, and the electronic interaction between the particles.[7,21,23−26]

The diffusion of the molecules cannot be treated as if it takes place in an isotropic continuum. Because electron transfer occurs over a relatively short range (< ∼10 Å), the structures of the first few solvent shells surrounding a donor play an important role in determining the spatial distribution of acceptors about a donor.[7,21] Diffusion is constrained by the fact that the equilibrium distribution of acceptor molecules must follow the solvent's radial distribution function, $g(r)$. As a result, molecular diffusion occurs within a potential of mean force ($-\ln[g(r)]$) rather than freely.[27,28] The effects are strongest within the first solvent shell. In addition, as a donor and acceptor approach each other, the effective diffusion constant is reduced.[7,21] The reduction of the diffusion constant on close approach is called the hydrodynamic effect,[29,30] and it is included in the theory via a distance-dependent diffusion constant, $D(r)$.

The influences of distance dependent transfer rate, diffusion, the radial distribution function, and the hydrodynamic effect have been incorporated into the theory of electron transfer in solution[7,8,21] as well as into the theory for electron transfer for donors and acceptors in the headgroup regions of micelles.[11,31] Experimental tests of the theoretical description of electron transfer in liquids[21] and in micelles[31,32] have taken place on a 50−100 ps to a few ns time scale. The results have shown good agreement between theory and experiment on these time scales.

† Current address: Softmatter Nanotechnology and Advanced Spectroscopy Group, Chemistry Division, Los Alamos National Laboratory, Los Alamos, NM 87545.

‡ Permanent address: Nanophotonics Laboratory, RIKEN, Hirosawa, Wako-shi, Saitama 351-0198, Japan.

10.1021/jp049391k CCC: $27.50
Published on Web 07/21/2004

The previous experiments used time dependent fluorescence spectroscopy that monitored the decay of the donor fluorescence. The theory calculates the time dependence of the excited-state population decay as a function of acceptor concentration.

In this paper, we extend the previous experiments to much shorter times (~200 fs). In the experiments, Rhodamine 3B cation ($R3B^+$) in low concentration is excited. Dimethylanaline (DMA) in high concentration can transfer an electron to $R3B^+$ to yield the R3B neutral radical and DMA^+. Because $R3B^+$ is in low concentration, and it is the species that is excited, we consider it to be the donor; that is, it is a hole donor, and DMA is a hole acceptor. Following excitation of the $R3B^+$, the time dependence is monitored using a broad continuum probe pulse. Spectra are recorded from 380 to 660 nm. In the absence of acceptors, the spectrum of excited $R3B^+$ is dominated by the ground-state bleach at ~570 nm and an excited-state absorption at ~445 nm. On the red side of the spectrum, in the region in which fluorescence occurs (>600 nm), the transient absorption spectrum also displays stimulated emission. When the DMA acceptors are added, an additional feature appears in the spectrum following excitation of the $R3B^+$, the R3B (neutral radical) peak at ~430 nm. Subtraction of the $R3B^+$ transient absorption spectrum (no acceptors) from the $R3B^+$/DMA transient absorption spectrum at times after $t = 0$ yields the R3B neutral radical spectrum.

The time dependence of the R3B neutral radical spectrum cannot be used to monitor the forward electron-transfer kinetics because back transfer (geminate recombination) is occurring on the same time scale as the forward transfer. The amplitude of the R3B peak is proportional to the population of charge-transfer species, which involves the combined kinetics of forward transfer and geminate recombination.[7,22] The forward transfer kinetics can be obtained by monitoring the excited-state population, which decays because of electron transfer and the intrinsic lifetime of the excited state. The excited-state population can be monitored by observing the decrease with time of the $R3B^+$ simulated emission in the spectral region (620 nm).

In the experiments presented below, time dependent stimulated emission is measured for a number of DMA concentrations. The time dependent decays are compared to the previously developed theoretical treatment of forward electron transfer in liquids.[7,21] Previous experiments on time scales longer than ~100 ps showed good agreement between theory and experiment.[21] Here, with better signal-to-noise ratios and a much wider range of times, we show that good agreement is obtained in some solvents, but in other solvents, there is significant deviation between experiment and theory. The solvents that agree with theory are a non-hydrogen-bonding solvent (acetonitrile) and mixtures of hydrogen-bonding alcohol solvents. Necessary input parameters for the calculations have been measured previously,[21] leaving only the contact electronic coupling matrix element, J_0, as an adjustable parameter with the assumption that the distance dependent fall off of the electronic interaction, β, in the Marcus theory[1−6] is ~1 $Å^{-1}$.[4,16,33−35] The data taken in three solvents are fit with the same value of J_0. In pure hydrogen-bonding solvents, such as ethanol and propylene glycol, the data do not fit nearly as well for any choice of J_0. However, by adjusting the hard sphere radius of the solvent, which modifies the spatial distribution of acceptors about a donor, it is possible to achieve good fits with the same value of J_0 used in the other solvents.

II. Experimental Procedures

Pump−probe experiments in which a particular wavelength is used for the pump and a continuum is used as the probe were performed using a Ti:sapphire regenerative amplified source and an optical parametric amplifier (OPA) and either a CCD detection system (broad band detection) or a lock-in amplifier system (narrow band detection). A double pass BBO OPA pumped by the output of the Ti:sapphire regenerative amplifier (800 nm, ~85 fs) was used to make 1.9 μm light. The left over 800 nm pulses were then summed with the ~1.9 μm pulses in another BBO crystal to produce the 565 nm pump pulses at a repetition rate of 1 kHz. 565 nm is on the red side of the $R3B^+$ absorption spectrum. The intensity of pump light was attenuated using a half-wave plate and polarizer combination. The pump energy (0.3−0.4 μJ/pulse) was chosen to make sure that the signal was linear in the pump intensity and that there was no sample degradation. All measurements described here were performed at the magic angle between the pump and probe beams.

A "white light" continuum, used for the probe, was generated by focusing 1−2 μJ of 800 nm light onto the back surface of a rotating CaF_2 crystal. A half-wave plate/polarizer combination was used to attenuate the 800 nm to give the most stable white light. Rotation was necessary to avoid rapid damage to the CaF_2. Use of CaF_2 with the 800 nm pump permitted the continuum to be generated from the near-IR to somewhat to beyond 380 nm. The white light was separated into two beams by a beam splitter. One beam was used as the probe crossed with the pump in the sample, and the other one, which passed through an unpumped spot in the sample, was used as a reference to monitor the intensity and spectral characteristics of the white light. Probe and reference beams were collimated and then focused by two off axis parabolic mirrors. The pump and probe beams had the spot sizes of about 100 and 50 μm, respectively. The delay between the pump and probe was achieve by passing the pump beam down two delay lines, a high-resolution delay with ~1 fs resolution and a long low resolution delay (~1 ps) that produced a maximum delay of ~12 ns.

The probe and the reference beams, after passing through the sample, were focused into two optical fibers by two microscope objectives. The outputs of the fibers are at the entrance slit of a 0.3 m monochromator with a 300 line/mm. The dispersed outputs of the two input beams are detected by a 1340 × 100 pixel CCD detector. The probe and the reference produce separately readout stripes on the CCD, which are used to obtain the difference absorption spectrum between pump on and pump off. The reference spectrum permits correction for variation over time of the white light characteristics.

In an alternative detection configuration, the probe and reference beams were directed out an exit slit on the monochromator rather than into the CCD. Two photomultiplier tubes (PMT) were used after the exit slit to measure the probe and reference signals at a selected wavelength. Signals from the PMTs were obtained by two gated integrators, and the probe signal was divided by reference signal using an analogue processor. The ratio was fed to a lock-in amplifier that detected the signal at 500 Hz. A mechanical chopper blocked every other pump pulse, resulting in a difference signal at 500 Hz.

Time resolution of the system, that is the cross-correlation between the pump pulse and the white light probe pulse, was determined by fitting the rising edge of the pump−probe signal of $R3B^+$ in ethanol solution to be ~150 fs. The shift in the position of the rising edge as a function of wavelength was used to determine the influence of chirp of the white light on the time dependence measured at different wavelengths.

All data were taken at room temperature 21 °C. All solvents were the highest grade commercially available and were used

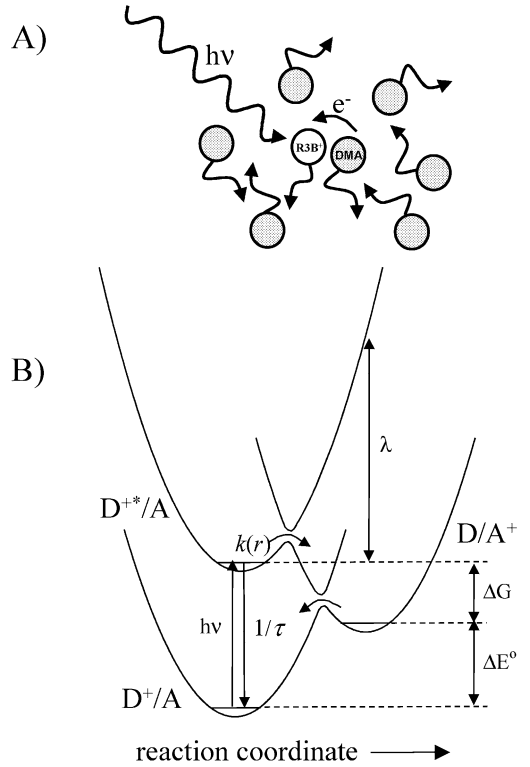

Figure 1. (A) Schematic of the experimental sample. $R3B^+$ is photoexcited and an electron transfers from one of the nearby DMAs in solution. The species are undergoing spatial diffusion, and their distribution is determined by the radial distribution function. (B) Schematic of the energy states and the kinetics. D^+ is the $R3B^+$ "hole donor". A is the DMA "hole acceptor".

as received. The cells were made of fused silica and had 1 mm path length. Each sample contained 0.05 mM $R3B^+$ (Exciton). DMA (Aldrich, 99.5+%) was used as received. Samples were degassed by several freeze-pump-throw cycles and sealed under vacuum. Optical absorption measurements were performed before and after evacuation and sealing of the samples to ensure the concentrations remained unchanged. All samples were stored in the dark. No measurable changes in the absorption spectra and the transient spectra were observed over a period of more then one year.

III. Theory and Data Analysis

The problem of photoinduced electron transfer between $R3B^+$ and DMA is illustrated in Figure 1. $R3B^+$ in low concentration is photoexcited. As shown in Figure 1A, the $R3B^+$ and high concentration DMA molecules are diffusing in a solvent. An electron can transfer from a DMA to the $R3B^+$ to yield the neutral R3B and a DMA^+. Although an electron is transferred from DMA to $R3B^+$, to be consistent with the terminology used in the development of the theoretical treatment,[7,21,22] $R3B^+$ will be referred to as the donor (D^+) because it is in low concentration and it is photoexcited. $R3B^+$ is a hole donor and DMA is a hole acceptor (A). Figure 1B is a schematic of the energy states and the kinetics. The system begins in the ground state (D^+A) and is photoexcited to $D^{+*}A$. The system can return to the ground state without electron transfer with a rate $1/\tau$, where τ is the lifetime measured in the absence of acceptors. Forward electron transfer can take place with the distance dependent rate $k(r)$ to the charge transfer state, DA^+. The system can return to the ground state via back electron transfer from the charge transfer state DA^+ to D^+A. The dynamics of back transfer[7,22,25,26,36,37] will be discussed in a subsequent publication. For the purposes of this paper, it is sufficient to note that back transfer is quite rapid, with essentially complete recombination occurring on a time scale that is very short compared to the experimental repetition rate. Therefore, the system is in the same initial state prior to each laser excitation. The free energy difference between the ground state and the charge transfer state is the difference in donor/acceptor redox potentials, $\Delta E°$. The free energy difference between the excited state and the charge transfer state is ΔG, the free energy associated with electron transfer. λ is the reorganization energy.[1−6]

The statistical mechanics theory of forward electron transport permits calculation of the experimental observable, the excited-state survival probability $\langle P_{ex}(t)\rangle$. $\langle P_{ex}(t)\rangle$ is the probability that a donor, excited at $t = 0$, is still excited at a later time, t. The ensemble-averaging technique, which has been derived previously, relates the observables to the two particle survival probability.[7,21,22] The result is

$$\langle P_{ex}(t)\rangle = \exp(-t/\tau)\exp(-4\pi C\int_{R_m}^{\infty}[1 - S_{ex}(t|R_0)]g(R_0)R_0^2\,dR_0) \quad (1)$$

where τ, C, and R_m denote respectively the donor fluorescence lifetime, the acceptor concentration, and the donor−acceptor contact distance (sum of their radii). $g(R_0)$ is the appropriate donor/acceptor radial distribution function.[8,23] $S_{ex}(t|R_0)$ is the probability that the donor is still excited at time t for a system in which there is only one acceptor located at R_0 at $t = 0$. $S_{ex}(t|R_0)$ satisfies the differential equation, with associated initial and boundary conditions.

$$\frac{\partial}{\partial t}S_{ex}(t|r_0) = L_{r_0}{}^{+}S_{ex}(t|r_0) - k_f(r_0)S_{ex}(t|r_0) \quad (2)$$

$$S_{ex}(0|R_0) = 1$$
$$4\pi R_0^2\frac{\partial}{\partial R_0}S_{ex}(t|R_0)|_{R_0=R_m} = 0 \quad (3)$$

$L_{r_0}{}^{+}$ is the adjoint of the Smoluchowski operator:[38,39]

$$L_{r0}{}^{+} = \frac{1}{r_0^2}\exp(V(r_0))\frac{\partial}{\partial r_0}D(r_0)r_0^2\exp(-V(r_0))\frac{\partial}{\partial r_0} \quad (4)$$

where $V(r_0) = -\ln(g(r_0))$ is the potential of the mean force, and $D(r_0)$ is the distance dependent diffusion constant.[23,28]

For electron transfer in the normal region ($-\Delta G < \lambda$), a widely used form of $k(r)$ was developed by Marcus:[1−6]

$$k(r) = \frac{2\pi}{\hbar\sqrt{4\pi\lambda(r)k_BT}}J_0^2\exp\left(\frac{-(\Delta G(r) + \lambda(r))^2}{4\lambda(r)k_BT}\right)\times \exp(-\beta(r - r_m)) \quad (5)$$

where reorganization energy (see Figure 1B) is given by

$$\lambda(r) = \lambda_i + \lambda_0 = \lambda_i + \frac{e^2}{8\pi\epsilon_0}\left(\frac{1}{\epsilon_{op}} - \frac{1}{\epsilon_{st}}\right)\left(\frac{1}{r_d} + \frac{1}{r_a} - \frac{2}{r}\right) \quad (6)$$

λ_i, the inner sphere reorganization energy can be calculated[4,40] and measured.[41,42] In general, $\lambda_o \gg \lambda_i$, and λ_i has no distance dependence. Therefore, for the experiments described in this paper, which involve the distance dependence of electron transfer, λ_i is expected to have a relatively small effect on the results. Here $\lambda_i = 0.10$ eV based on values for similar molecules.[21,40,41] ϵ_{op} and ϵ_{st} are the high frequency and static

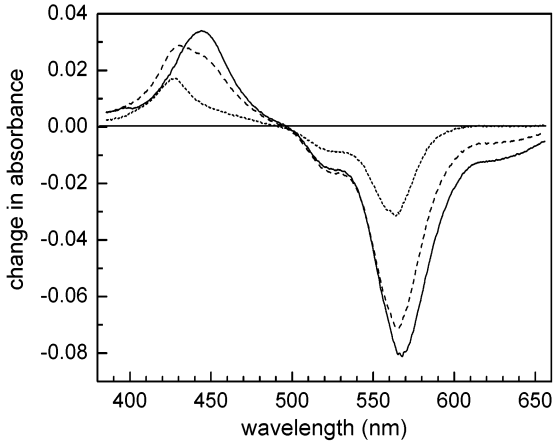

Figure 2. Pump-probe difference spectra at 8 ps delay in propylene glycol. The solid curve is $R3B^+$ taken with no DMA acceptors. The dashed curve is the spectrum with a DMA acceptor concentration of 0.3 M. A new feature at ~430 nm arises from the generation of the R3B neutral radical via electron transfer from a DMA. The dotted curve results from subtracting the solid curve from the dashed curve. The R3B neutral radical spectrum is the peak at ~430 nm.

dielectric constants, respectively; r_d and r_a are the donor and acceptor hard sphere radii. The values of these four parameters for the solvents, and the donor and acceptor studied here have been reported previously. [21] $\Delta G(r)$ is the free energy change due to forward transfer (see Figure 1B). e, $\hbar$, and k_B are the fundamental charge, Planck's, and Boltzmann's constants, respectively. The J_0 and β parameters characterize the magnitude and distance dependence of the transfer rate, respectively. We assume $\beta = 1$ Å^{-1} because β has been found to be ~1 Å^{-1} in many studies.[4,16,33−35] In addition, previous electron-transfer measurements on the donor and acceptor studied here indicate that $\beta \cong 1$ Å^{-1}.[21] However, the value of β will be discussed further below.

IV. Results and Discussion

Figure 2 displays three pump−probe difference spectra taken with the CCD. The solvent is propylene glycol and the probe delay is 8 ps. The solid curve is for $R3B^+$ taken with no DMA acceptors in the solution. The negative going peak at ~570 nm is the ground-state bleach. The positive going peak at ~445 nm is an excited-state−excited-state absorption. The broad low amplitude negative going feature to the red of ~600 nm is stimulated emission induced by the probe. The lifetime varies somewhat with solvent. The dashed line in Figure 2 shows the spectrum with an acceptor concentration of 0.3 M. A new feature is evident at ~430 nm. This feature can be identified as the R3B neutral radical generated via electron transfer from a DMA (see below). The region of stimulated emission, which reflects the $R3B^+$ excited-state population, has decreased by ~50%. However, the ground-state bleach has decreased much less. Forward electron-transfer quenches the excited-state population, but the ground-state bleach does not recover until electron back transfer has occurred to regenerate $R3B^+$.

To obtain a spectrum of the R3B neutral radical, it is necessary to subtract off the excited state−excited-state absorption band. The excited state−excited-state absorption has an amplitude that is proportional to the stimulated emission band because they are both determined by the number of excited states. Therefore, the R3B spectrum is obtained by subtracting the no acceptor spectrum (solid curve) from the spectrum with acceptors (dashed curve) after scaling it to the spectrum with acceptors in the region of the stimulated emission. The resulting spectrum (dotted curve) shows the R3B neutral radical in the region around ~430 nm. This spectrum coincides with the spectrum of R3B taken using pulsed radiolysis to produce the neutral radical.[43] The appearance of the R3B neutral radical spectrum demonstrates that the change in dynamics when DMA is added to the solutions arises from electron transfer. We can estimate the extinction coefficient of the R3B neutral radical by comparing the amplitude of the signal at 430 nm to that of the ground-state bleach at 564 nm. The result is ~3×10^4 M^{-1} cm^{-1}, which is close to the reported value.[43] We were unable to observe the DMA^+ absorption. From the literature it is known that it is maximum at 470 nm with an extinction coefficient of ~25×10^3 M^{-1} cm^{-1} in aqueous solutions. In the dotted spectrum in Figure 2, the DMA^+ would have an absorbance of ~0.0005 and would be obscured by the R3B neutral radical absorption. The spectra displayed in Figure 2 are virtually identical in the solvents studied.

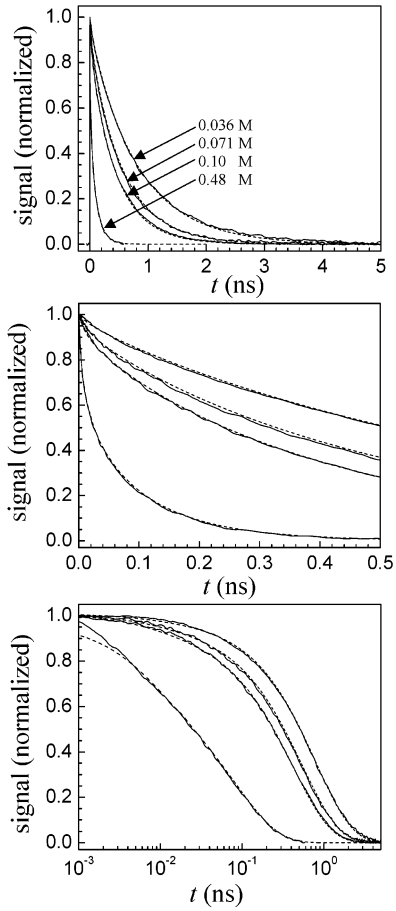

Figure 3. Electron-transfer data and calculations for four DMA concentrations in acetonitrile. Top panel: times out to 5 ns. Middle panel: expanded time scale out to 0.5 ns. Bottom panel: linear amplitude but log time scale to make it possible to see the data and fits over all times, particularly at short time. The calculations have one adjustable parameter, J_0.

Figure 3A displays linear plots of stimulated emission data (620 nm) taken in the solvent acetonitrile for four concentrations of the DMA acceptor, 0.034, 0.067, 0.10, and 0.48 M (top to bottom, solid curves). In addition to the data, the figure displays the best fits to the data (dashed curves) using a single adjustable parameter, J_0. β was fixed at 1 Å^{-1} as discussed at the end of section III. All of the other parameters were fixed at the values determined previously.[21] In contrast to previous experiments that covered a time range beginning at >50 ps,[21] here the data extend to a factor of ~100 shorter times. Figure 3B is a blow up of

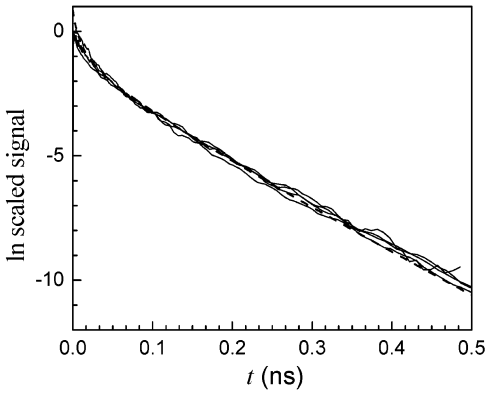

Figure 4. Data from Figure 3 showing that the concentration scaling relationship predicted by eq 7 is obeyed.

the short time portion of the data out to 500 ps with the fits. To see the full range of the data and comparison to the fits more clearly, Figure 3C displays the same data and fits with the horizontal axis being log *t*. Note that the vertical scale is linear, so that a log scale for the amplitude does not mask deviations between theory and experiment. Although the agreement between theory and experiment is not perfect, the agreement is very good over a time range of ~4 decades. The worst agreement is for the very short time portion of the highest concentration. There is only one adjustable parameter, $J_0 = 200$ cm^{-1}. This same value is used in describing the electron transfer in the other solvents discussed below. In prior experiments on this system, the data were fit with $J_0 = \sim 300$ cm^{-1}. However, in those experiments the time range covered was ~2 decades less and the signal-to-noise ratio was considerably worse. Furthermore, a narrower range of DMA acceptor concentration was used.

As a further test of the agreement with theory, the acetonitrile data shown in Figure 4 is replotted using a concentration scaling relation. As can be seen in eq 1, the electron-transfer portion of $\langle P_{ex}(t)\rangle$ scales exponentially with the concentration, *C*. In Figure 4, the contribution form the $R3B^+$ excited-state lifetime was removed from the data, and all of the curves were scaled to an acceptor concentration of 1 M. The scaling relation is

$$\frac{1}{C}\left(\ln(P_{ex}) + \frac{t}{\tau}\right) = -4\pi\int_{R_m}^{\infty}[1 - S_{ex}(t|R_0)]g(R_0)R_0^{\,2}\,dR_0 \quad (7)$$

The rhs of eq 7 is independent of concentration. Because the data for different concentrations have different decay rates, the convolution with the instrument response results in different peak amplitudes of the curves. Therefore, the curves were also normalized. The theoretical curve (dashed curve in Figure 4) was not convolved with an instrument response. Its amplitude was matched slightly after $t = 0$. The scaling relationship is seen to hold quite well. Because the scaling depends on the exponential of the concentration, even small errors in the determination of the sample concentration can lead to noticeable errors in the scaling.

Figure 5 displays data for $R3B^+$ and 0.1 M DMA in two solutions that are mixtures of hydrogen-bonding solvents, 50/50 v/v ethylene glycol/ethanol and 58/42 v/v propylene glycol/2-butanol. In addition to the data in the two solvents, calculated curves are shown. The calculated curves were obtained *without recourse to adjustable parameters*. The value of $J_0 = 200$ cm^{-1} found from the experiments on acetonitrile (Figure 3) was used. Because J_0 is the electronic matrix element at the contact distance between the donor and acceptor, its value should be essentially independent of the solvent. There are a large number

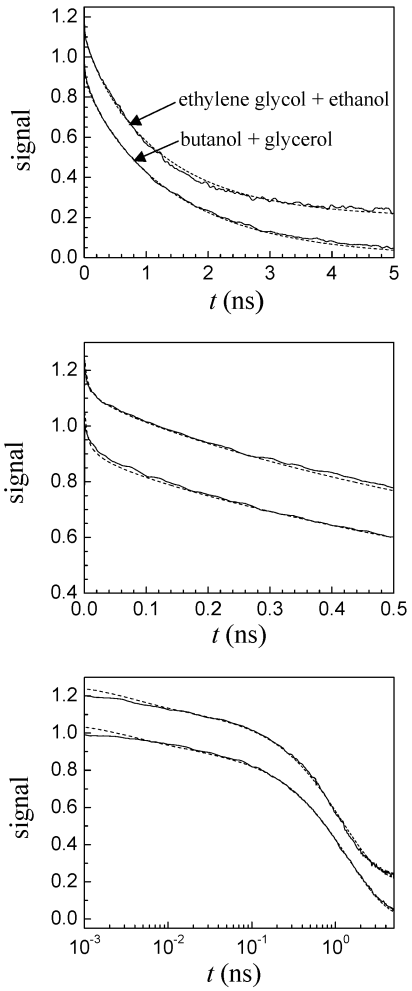

Figure 5. Data and calculations in two solvents. The calculated curves employ *no adjustable parameters*.

of input parameters in the calculations that depend on the solvent. They are the optical and static dielectric constants, the diffusion constants, the solvent hard sphere radius (taken as the average for mixtures) that determines the radial distribution function, and the difference in the donor acceptor redox potentials (used to determine ΔG_0). These inputs are known from independent measurements.[21] In addition, the donor and acceptor radii, the inner sphere reorganization energy,[21] and the Marcus theory β and J_0 are input parameters. While not perfect, theory and experiments agree for almost 4 decades in time without adjustable parameters. In both liquids, some deviation can be seen in the bottom panel for times < ~10 ps, but the deviations are small. The theory accounts for the distance dependence of the electron transfer in systems in which the donor and acceptors are undergoing diffusive motion. However, the spatial dependence of the acceptors about a donor and the diffusion of the donors and acceptors are not described in terms of a featureless continuum. The spatial distribution and the diffusion are described in terms of a structured solvent in which the structure is brought in through the radial distribution function.

The theory and experiments agree quite well in both the non-hydrogen-bonding solvent, acetonitrile, and in the hydrogen-bonding solvents that are mixtures of mono and polyalcohols. However, the situation is different for experiments conducted in pure hydrogen-bonding alcohol solvents, ethanol, propylene glycol, and ethylene glycol. The calculations with no adjustable parameters show deviations from the data, particularly at short

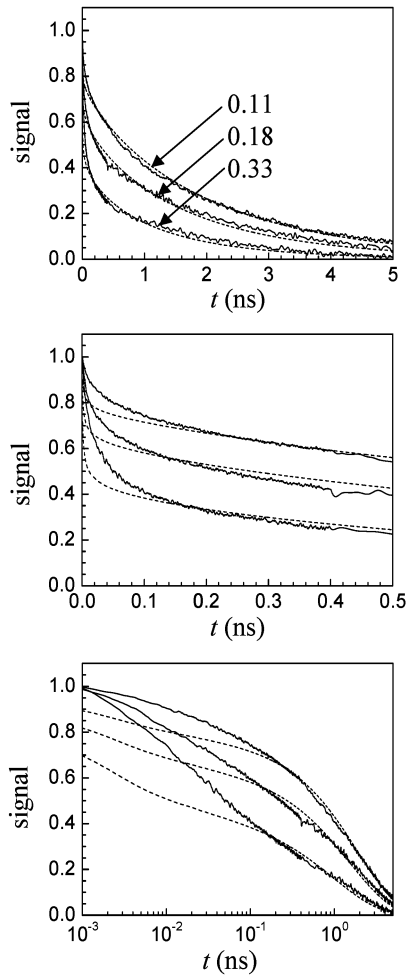

Figure 6. Electron-transfer data and calculations for three DMA concentrations in propylene glycol. Top panel: times out to 5 ns. Middle panel: expanded time scale out to 0.5 ns. Bottom panel: linear amplitude but log time scale to make it possible to see the data and no adjustable parameter calculations over all times. Unlike the data and calculations in Figures 3 and 5, the agreement at short time is not good. This is particularly evident in the bottom panel.

time. The deviations are mild for ethanol, but quite large for propylene glycol and even greater for ethylene glycol. Figure 6 displays the propylene glycol data and calculations for three concentrations. The deviations from the calculation become significant for times $< \sim$200 ps. In previous experiments on $R3B^+$/DMA in propylene glycol that had a time resolution of $\sim$100 ps, some deviations were noted,[21] but the lack of time resolution did not make it possible to see the full extent of the deviations from theory.

As with the data presented above, all of the input parameters except J_0 and β are known. Varying the input parameters around their measured values[21] to account for the error bars on the parameters did not improve the agreement. In particular, the diffusion constants were varied for the three pure alcohols, but the agreement between calculation and theory was not improved. Furthermore, it was found that adjusting J_0 could not improve the agreement. By making J_0 very large, the short time agreement was improved at the expense of poor fits at longer times.

One possible explanation for the disagreement is that the DMA aggregates with the $R3B^+$ or with itself. This seems unlikely because of the agreement in the mixtures of the alcohol solvents. Nonetheless, this possibility was examined in detail. First, the scaling of the data at different concentrations was tested using eq 7 as in Figure 4. Aggregation would be a nonlinear function of concentration. Therefore, the scaling relation given in eq 7 would not be obeyed. It was found that the data for the pure alcohols did scale properly, indicating a lack of aggregation. In addition, in a previous study of $R3B^+$/DMA in ethylene glycol,[44] the solvent in which the greatest deviation from theory is observed, absorption spectra of R3B were taken as a function of DMA concentration, with the DMA concentration ranging from 0 to 0.3 M. No changes were observed in the absorption spectrum that would suggest specific aggregation.

To further test the possibility that aggregating is responsible for the form of the data, calculations were performed that included acceptor aggregation about the donor.[44] To model acceptor aggregation, the radial distribution function was modified by increasing the first peak (the peak representing the first shell about the $R3B^+$) in height while keeping the total radial distribution function normalized. In addition, lower bulk DMA concentrations were tried, to account for decreased available concentration resulting from aggregation. Increasing the first peak placed more DMA molecules close to the $R3B^+$ than would occur without a specific attractive interaction between donor and acceptor. The increased local concentration caused the short time portion of the decays to become faster, but the shapes of the curves were not consistent with the data for any possible DMA concentrations, regardless of the height of the first peak in the radial distribution function. The $R3B^+$ is too low in concentration to aggregate itself. Aggregation in Rhodamine dyes occurs at concentrations above $\sim 3 \times 10^{-3}$ mol/L.[45] Detailed electronic absorption studies of the DMA from low concentration to the high concentration were performed.[44] No changes in the optical absorption was observed between low and high concentration, indicating that DMA is not aggregating. All of these results demonstrate that aggregation does not account for the unusual experimental results observed in the pure alcohols.

Variation of either of two parameters, β and the hard sphere solvent radius (the radial distribution function, $g(r)$), could bring the data and the calculated curves into agreement. To achieve agreement by varying β, it was necessary to have $\beta = \sim 0.7$ $Å^{-1}$. This is a large change in β. The value is outside of the range that would be expected for the type of system under study.[4,16,33−35] In addition, there is an argument that a value of β other than ~ 1 $Å^{-1}$ is not responsible for the deviation between the calculated curves and the experimental data that is more compelling than the numerical value of β required to fit the data. In the mixtures of ethylene glycol and ethanol, $\beta = 1$ $Å^{-1}$ produced calculated curves that fit the data quite well with no adjustable parameters. β reflects the fall off of the electronic coupling between donor and acceptor with distance. It seems exceedingly unlikely that the value of $\beta = 1$ $Å^{-1}$ that is appropriate for the ethanol/ethylene glycol mixture will be substantially different in the individual pure solvents, ethanol and ethylene glycol. The value of β is the same in acetonitrile and in the mixtures of butanol/glycerol and ethylene glycol/ethanol, demonstrating that the difference does not arise for a single component solvent vs a mixture and does not depend on which mixture of alcohols is used. The lack of agreement between the calculations and data only occurs for single component hydrogen-bonding solvents.

It has been shown for hard sphere liquids that a solute's spatial distribution follows the solvent's radial distribution function, $g(r)$.[46] The donor and acceptors are not in high enough concentration to independently form a structured distribution; under

normal circumstances, it is assumed that they follow the structure determined by the solvent molecules.[46] This is the basic assumption that is used in describing the spatial distribution of acceptors about a donor. The distribution of acceptor molecules about a donor can be modeled using the solvent $g(r)$. It is assumed, as in the hard sphere simulations, that acceptor solutes track the single molecule solvent $g(r)$. Electron transfer calculations that compared results using a hard sphere radial distribution function to a radial distribution function obtained experimentally with neutron scattering showed that the differences were negligible.[8] That is, the use of a hard sphere $g(r)$ distribution function rather than, for example, a Lennard-Jones $g(r)$, is an adequate model of the liquid.

In a previous electron transfer study for the $R3B^+$/DMA electron-transfer system in ethylene glycol, a similar inability to fit the data using the theory employed here was reported.[44] As noted above, the previous electron-transfer studies on $R3B^+$/DMA did not cover as broad a range of times and did not have as good signal-to-noise ratios. In that work,[44] the calculations were modified by using the solvent hard sphere radius, which determines the hard sphere radial distribution function, $g(r)$, as an adjustable parameter. By increasing the solvent hard sphere radius substantially, the data could be fit over the range of times studied.

The basic idea of increasing the hard sphere radius is to account for the possibility that in the pure hydrogen-bonding liquids the acceptor concentration does not track the single molecule solvent $g(r)$. Figure 7 displays the same data shown in Figure 6 but with calculations in which the hard sphere radius was treated as an adjustable parameter. All of the other parameters are fixed at the values appropriate for propylene glycol with $J_0 = 200\ \text{cm}^{-1}$ and $\beta = 1\ \text{Å}^{-1}$, as found from the experiments in acetonitrile (Figures 3 and 4) and confirmed by the experiments on the mixtures, ethylene glycol/ethanol and butanol/glycerol (Figure 5). While the agreement is certainly not perfect, it is far superior to the calculations presented in Figure 6. For the two lower concentrations, the agreement is quite reasonable. For the highest concentration significant deviation is observed at <6 ps. In ethanol, in which the deviations are small, changing the hard sphere radius produces very good agreement. In ethylene glycol, the agreement is similar to that obtained for the experiments in propylene glycol.

The single molecule hard sphere radii of ethanol, propylene glycol, and ethylene glycol are 2.07, 2.36, and 2.17 Å, respectively.[21,44] The ratios of the values used to fit the data to the single molecule hard sphere radii for ethanol, propylene glycol, and ethylene glycol are 1.7, 2.9, and 3.5, respectively. For comparison, in the previous study of this anomalous behavior in ethylene glycol, the ratio was also found to be 3.5.[44] These results suggest that the assumption that solute's track the single molecule solvent $g(r)$ in pure hydrogen-bonding liquids is not valid.

Ethanol forms hydrogen-bonding chains by making two hydrogen bonds. Almost all of the hydroxyl's are both hydrogen-bonding donors and acceptors. This is also true of polyalcohols like propylene glycol and ethylene glycol. However, in polyalcohols, the hydrogen-bonding is more extensive than in monoalcohols because each of the hydroxyls of a polyalcohol forms two hydrogen bonds. Thus, the polyalcohols form hydrogen-bonding networks, while the monoalcohols can only from chains. If the monoalcohols were envisioned as polymer chains, and the polyalcohols were envisioned as crossed liked polymer chains, it is clear that a solute would not track the monomer radial distribution function. However, hydrogen-bonding networks are not polymers. Hydrogen bonds are constantly breaking and being formed. The networks are dynamics with continually evolving structures. Nonetheless, the results indicate that the hydrogen-bonded structures influence the DMA solutes radial distribution function with respect to the $R3B^+$. In going from ethanol to propylene glycol, to ethylene glycol, the number of hydroxyls per carbon increases, resulting in fewer methyl groups per hydrogen bond to disrupt the structure. This may be the reason that the deviation from the single solvent hard sphere radius required to improve the fits to the data increases as the percentage of methyl groups in the solvent decreases. The mixtures (Figure 5) do not require changes in the average hard sphere radii to obtain agreement with the calculation using no adjustable parameters. Although highly hydrogen-bonding, the mixtures will have a high degree of local structural disorder. It is possible that the local disorder is the reason that the DMA solute does track the solvent radial distribution function in the mixtures. However, there are some deviations at short time in Figure 5. This may be a hint of the major deviations seen in Figure 6.

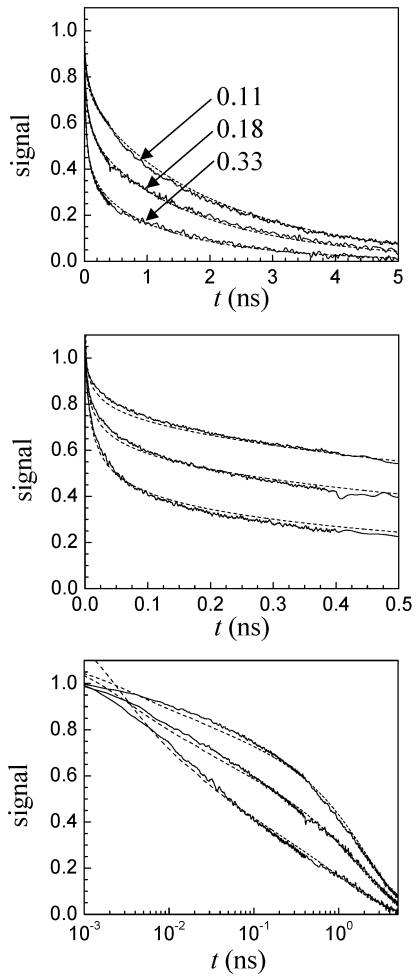

Figure 7. Electron-transfer data and calculations for three DMA concentrations in propylene glycol. Top panel: times out to 5 ns. Middle panel: expanded time scale out to 0.5 ns. Bottom panel: linear amplitude but log time scale to make it possible to see the data and over all times. The calculations use one adjustable parameter, the solvent hard sphere radius. The agreement between the data and calculations is substantially improved compared to Figure 6 (see text).

V. Concluding Remarks

Experiments and calculations have been presented that examined photoinduced electron transfer between a photoexcited

donor $R3B^+$ (hole donor) and various concentrations of the acceptor DMA (hole acceptor) in six liquid solutions. The R3B radical produced by forward electron transfer was observed, confirming that electron transfer influences the excited-state population dynamics in the $R3B^+$/DMA system. Stimulated emission was used to monitor the time dependence of forward electron transfer. The data spanned a time range from subpicosecond to many nanoseconds.

The experimental data were compared to a statistical mechanical theory that describes electron transfer in liquid solution.[7,21,23−26] The theory includes diffusion in the liquid that is described in terms of a radial distribution function rather than as a featureless continuum. In addition the theory includes the distance dependence of the diffusion process (hydrodynamic effect). The large number of input parameters for the theory are known,[21] which left only on adjustable parameter, the magnitude of the electronic interaction at contact, J_0. J_0 was found to be 200 cm^{-1} by fitting data in acetonitrile. Then, with *no adjustable parameters*, good agreement was obtained between data and calculations in two other liquids. However, in three pure hydrogen-bonding liquids, it was found that agreement could only be achieved if the hard sphere radius used in the determination of the radial distribution function of the acceptors about a donor was increased over that which is appropriate for a single solvent molecule. It was suggested that in contrast in the hard sphere simulations, in hydrogen-bonded network liquids, solute molecules do not track the solvents radial distribution function.[46]

The work presented here sets the stage for studying geminate recombination following forward electron transfer in these same systems and investigating the probability that the radical formed by forward electron transfer will escape geminate recombination. A recent study of $R3B^+$ in pure DMA solvent has shown very rapid forward electron transfer (∼0.5 ps time scale) followed by much slower geminate recombination (∼25 ps time scale), and a small percentage of radicals that escape geminate recombination.[47] Forward photoinduced electron transfer and recombination in liquids and micelles are currently under investigation.

Acknowledgment. We thank Ilya Finkelstein for his considerable help in the computer programming associated with the experimental apparatus. This work was supported by the Department of Energy (DE-FG03-84ER13251).

References and Notes

(1) Marcus, R. A. *J. Chem. Phys.* **1956**, *24*, 966.
(2) Marcus, R. A. *J. Chem. Phys.* **1956**, *24*, 979.
(3) Marcus, R. A. *Annu. Rev. Phys. Chem.* **1964**, *15*, 155.
(4) Marcus, R. A.; Sutin, N. *Biochim. Biophys. Acta* **1985**, *811*, 265.
(5) Sutin, N. Nuclear and Electronic Factors in Electron Transfer: Distance Dependence of Electron-Transfer Rates. In *Electron Transfer in Inorganic, Organic, and Biological Systems*; Bolton, J. R., Mataga, N., McLendon, G., Eds.; American Chemical Society: Washington, DC, 1991; p 25.
(6) Bolton, J. R.; Archer, M. D. Basic Electron-Transfer Theory. In *Electron Transfer in Inorganic, Organic, and Biological Systems*; Bolton, J. R., Mataga, N., McLendon, G., Eds.; American Chemical Society: Washington, DC, 1991.
(7) Weidemaier, K.; Tavernier, H. L.; Swallen, S. F.; Fayer, M. D. *J. Phys. Chem. A* **1997**, *101*, 1887.
(8) Swallen, S. F.; Weidemaier, K.; Tavernier, H. L.; Fayer, M. D. *J. Phys. Chem.* **1996**, *100*, 8106.
(9) Burel, L.; Mostafavi, M.; Murata, S.; Tachiya, M. *J. Phys. Chem. A* **1999**, *103*, 5882.
(10) Iwai, S.; Murata, S.; Tachiya, M. *J. Chem. Phys.* **1998**, *109*, 5963.
(11) Tavernier, H. L.; Barzykin, A. V.; Tachiya, M.; Fayer, M. D. *J. Phys. Chem. B* **1998**, *102*, 6078.
(12) Weidemaier, K.; Tavernier, H. L.; Fayer, M. D. *J. Phys. Chem. B* **1997**, *101*, 9352.
(13) Aota, H.; Araki, S.; Morishima, Y.; Kamachi, M. *Macromolecules* **1997**, *30*, 4090.
(14) Borsarelli, C. D.; Cosa, J. J.; Previtali, C. M. *Photochem. Photobiol.* **1998**, *68*, 438.
(15) Hackett, J. W. I.; Turro, C. *J. Phys. Chem. A* **1998**, *102*, 5728.
(16) Gray, H. B.; Winkler, J. R. *Annu. Rev. Biochem.* **1996**, *65*, 537.
(17) Hu, Y. Z.; Tsukiji, S.; Shinkai, S.; Oishi, S.; Hamachi, I. *J. Am. Chem. Soc.* **2000**, *122*, 241.
(18) DiBilio, A. J.; Dennison, C.; Gray, H. B.; Ramirez, B. E.; Sykes, A. G.; Winkler, J. R. **1998**.
(19) Langen, R.; Chang, I.-J.; Germanas, J. P.; Richards, J. H.; Winkler, J. H.; Gray, H. B. *Science* **1995**, *268*, 1733.
(20) Murata, S.; Nishimura, M.; Matsuzaki, S. Y.; Tachiya, M. *Chem. Phys. Lett.* **1994**, *219*, 200.
(21) Tavernier, H. L.; Kalashnikov, M. M.; Fayer, M. D. *J. Chem. Phys.* **2000**, *113*, 10191.
(22) Weidemaier, K.; Fayer, M. D. *J. Phys. Chem.* **1996**, *100*, 3767.
(23) Swallen, S. F.; Weidemaier, K.; Fayer, M. D. *J. Chem. Phys.* **1996**, *104*, 2976.
(24) Tachiya, M. *Radiat. Phys. Chem.* **1983**, *21*, 167.
(25) Lin, Y.; Dorfman, R. C.; Fayer, M. D. *J. Chem. Phys.* **1989**, *90*, 159.
(26) Dorfman, R. C.; Lin, Y.; Fayer, M. D. *J. Phys. Chem.* **1990**, *94*, 8007.
(27) Rice, S. A. *Diffusion-Limited Reactions*; Elsevier: Amsterdam, 1985.
(28) Northrup, S. H.; Hynes, J. T. *J. Chem. Phys.* **1979**, *71*, 871.
(29) Deutch, J. M.; Felderhof, B. U. *J. Chem. Phys.* **1973**, *59*, 1669.
(30) Zwanzig, R. *Adv. Chem. Phys.* **1969**, *15*, 325.
(31) Tavernier, H. L.; Laine, F.; Fayer, M. D. *J. Phys. Chem. A* **2001**, *105*, 8944.
(32) Weidemaier, K.; Tavernier, H. L.; Chu, K. T.; Fayer, M. D. *Chem. Phys. Lett.* **1997**, *276*, 309.
(33) Closs, G. L.; Miller, J. R. *Science* **1988**, *240*, 440.
(34) Miller, J. R.; Beitz, J. V.; Huddleston, R. K. *J. Am. Chem. Soc.* **1984**, *106*, 5057.
(35) Guarr, T.; McLendon, G. *Coord. Chem. Rev.* **1985**, *68*, 1.
(36) Burshtein, A. I. *Chem. Phys. Lett.* **1992**, *194*, 247.
(37) Burshtein, A. I.; Zharikov, A. A.; Shokhirev, N. V. *J. Chem. Phys.* **1992**, *96*, 1951.
(38) Smoluchowski, M. V. *Z. Phys. Chem.* **1917**, *92*, 129.
(39) Agmon, N.; Szabo, A. *J. Chem. Phys.* **1990**, *92*, 5270.
(40) Hale, J. M. The Rates of Reactions Involving Only Electron Transfer, at Metal Electrodes. In *Reactions of Molecules at Electrodes*; Hush, N. S., Ed.; Wiley-Interscience: New York, 1971; p 229.
(41) Liu, J. Y.; Bolton, J. R. *J. Phys. Chem.* **1992**, *96*, 1718.
(42) Markel, F.; Ferris, N. S.; Gould, I. R.; Myers, A. B. *J. Am. Chem. Soc.* **1992**, *114*, 6208.
(43) Beaumont, P. C.; Johnson, D. G.; Parsons, B. J. *J. Photochem. Photobiol. A: Chem.* **1997**, *107*, 175.
(44) Tavernier, H. L.; Fayer, M. D. *J. Chem. Phys.* **2001**, *114*, 4552.
(45) Lutz, D. R.; Nelson, K. A.; Gochanour, C. R.; Fayer, M. D. *Chem. Phys.* **1981**, *58*, 325.
(46) Throop, G. J.; Bearman, R. J. *J. Chem. Phys.* **1965**, *42*, 2408.
(47) Saik, V. O.; Goun, A. A.; Fayer, M. D. *J. Chem. Phys.* **2004**, in press.